

Hybrid Rocket Motor Ground Testing Results to Enable the Vision of Rapid Flight Testing for System Development

Paige K. Nardozzo, Justin R. Smith, Sarah H. Popkin, Joshua P. Higginson, Marcus P. Musser, Chuck E. Hebert, and Gary Worrell

ABSTRACT

The Johns Hopkins University Applied Physics Laboratory (APL) explored a reusable hybrid rocket design to enable low-cost, rapid flight testing. Rocket motor reusability requires addressing the unique thermal challenges of the combustion chamber. Specifically, APL focused on addressing an unexpected thermal load on the forward bulkhead that resulted in melted aluminum near the injector. Thermal management design concepts included changes to the forward bulkhead by adding insulation, lengthening the precombustion chamber, and adjusting the spray angle of the injector. The design study showed that both lengthening the precombustion chamber and using an axial injector with contoured ports resulted in adequate thermal management, confirming that aluminum is suitable for the hybrid rocket combustion chamber forward bulkhead in APL's design.

INTRODUCTION

Motivation

US adversaries continue to advance their militaries and weapons, putting the United States at risk of losing the military dominance it has enjoyed since World War II. This statement is not specific to hypersonic weapons, perhaps inferred from the title of this article, but encompasses many technology domains. Advances in tracking (radar and communications) reduce the effectiveness of strike weapons and the surprise of stealth, advances in defensive surface-to-air missiles challenge the survivability of both weapons and aircraft, and advances in long-range strike weapons not only put naval and ground assets at risk but also negate their utility. The United States will need to develop new systems to negate and counter these advances and increase its military capability, and it has prioritized

hypersonic research and systems as a way to maintain its superiority.

Effective research requires access to facilities and experimentation to prototype and learn. Over the past several decades, US adversaries have continued to develop new facilities, giving foreign researchers access to test facilities, while the United States has shuttered its own. Consequently, the United States now relies on a few older facilities, in combination with periodic flight testing, to develop new weapons. While the United States has made progress in new systems, it has come at great cost with long timelines, in part due to the limited availability of test facilities and in part due to the high costs of flight testing. Rising test costs build high test expectations, and any failure risks program cancellation,

resulting in longer timelines and higher costs to increase the probability of a successful flight. A recent Government Accountability Office report details cost overruns and extended schedules.¹

There is a national need to flight-test hypersonic technology earlier in the program life cycle to aid decisions and technology development before designs are locked in. While the United States has had success with individual flight tests, there is still significant risk in subsystem technology because of coupling (each subsystem affects the other). Individual uncoupled test campaigns (arcjet tests, wind tunnel tests, and ground tests) are not sufficiently effective risk mitigation methods for hypersonic systems, as flight environments cannot be perfectly duplicated on the ground. Furthermore, access to ground-test assets is limited as the fundamental research and weapons development communities compete with each other for ground testing. Consequently, flight tests—which are historically failure prone—offer the first exposure to combined flight environments for new hypersonic systems. Considering the significant cost and schedule to reach flight testing, this approach is undesirable and risky.

The current testing construct for most programs is to use a ground facility to evaluate a specific aspect of a test article. For example, material survivability in hypersonic conditions is challenging because of intense heating. To reduce risk, a material sample typically undergoes arcjet testing where it experiences significant heating for long durations. Unfortunately, surviving this test does not ensure material acceptability because arcjet tests do not duplicate the pressure and shear loads experienced in flight and do not include mechanical details like interfaces and seals that must also function. These challenges apply to all areas of a hypersonic system—antennas, control surfaces, sensors, electronics. All must work collectively and robustly to accomplish a successful mission.

Testing Limitations

While ground-test facilities offer extensive capabilities for hypersonic testing, key limitations reduce their effectiveness. Of the main facilities typical for ground testing, not a single one achieves all the needs based on runs per day—scale, Mach, pressure, temperature, turbulence, duration, and productivity. An additional challenge with ground testing is the overall limited access to facilities. Cost, competition, and regular maintenance all contribute to lack of on-demand availability. Every ground test becomes a compromise of testing needs versus testing constraints; consequently, the results of the test are not representative of flight. Consider the previously mentioned material example: Samples are exposed to high heat fluxes in arcjet facilities, but the pressures are low, creating much lower shear stresses—a significant limitation for coatings or ablation-type degradation risks. Additionally, arcjet test sample sizes are small, on

the order of inches, making it difficult to test flight size interfaces with seals and material stacks. The size/scale limitation makes it difficult to test risk reduction of the combined thermal-structural problem. Simply stated, the US community is currently unable to easily test large sample sizes for hypersonic applications. Flight testing is the other main option, but it comes with significant cost and schedule consequences. A “cheap” flight test using sounding rockets is still on the order of \$5–10 million and takes about a year of planning and execution to complete. Higher-profile demonstration flight tests are an order of magnitude higher in cost, and it typically takes 5+ years to accomplish a single flight test. Furthermore, when those tests occur, they often fail, causing extra delays or even program elimination. However, it is unfair to pass judgment on programs of the past, as their efforts were commensurate with the options available.

Today, solid rocket motors come in a variety of sizes and thrust profiles, and they are preferred over liquid engines because of their simplicity and reliability. Missions and payloads determine speed, direction, and altitude needs, which are then used to size a rocket. The net result is usually a rocket with one to three stages that has the highest probability for achieving the flight conditions desired. Minimal flight trajectory shaping is possible and is controlled by launch angles, actuators, and coast times. One of the significant limitations with a sounding rocket is that, once ignited, the thrust cannot be controlled, resulting in two main consequences:

1. Although it may be notionally predictable, the rocket trajectory is uncontrollable and based on launch angles and the delivered thrust of the motor.
2. The lack of thrust control severely constrains burn-out velocity and flight path angle, which limits payload insertion conditions.

Because of these limitations, many different motors are needed to achieve different flight conditions. Each motor must be designed, built, and qualified, adding cost and time. Instead of having a system that delivers the desired performance, the industry is forced to use what is available to the best degree possible.

Consequences

Considering the current status of ground testing facilities and the cost of flight testing, the hypersonic community is confined to a situation that stifles progress and avoids risks, sacrificing potential performance. Larger programs rely on decades-old techniques to solve current problems, requiring them to pursue multiple options or solutions, which adds significant cost. At the basic research level, scientists and engineers cannot test new technology in flight environments, amplifying the problem. The cumulative consequence is a high-risk posture across the technology disciplines for hypersonic applications.

There is a need for accessible lower-cost flight testing that is available at a rate equivalent with the needs of the community and that can be executed in a manner that accepts risks and failure—so programs, businesses, and academia can test in a manner that advances the state of the art in years, not decades. Instead of failures being feared, they should be seen as learning opportunities, with lessons implemented in weeks, not years, for subsequent flight attempts.

OUR SOLUTION

Our vision for hypersonic testing involves a flexible, reusable rocket that could test a variety of payloads in a variety of flight conditions. By facilitating rapid, inexpensive testing, programs could test their concepts early, allowing the engineering design process to take advantage of lessons learned without the pressure of the late-stage, expensive, and highly visible flight tests faced by current programs.

The test vision, illustrated in Figure 1, shows a rocket boosting to specific test windows and then returning for landing, which could also be located downrange. A reusable sounding rocket enables new capabilities that are not available with existing ground testing or flight testing using traditional solid rocket motors. First, a reusable system allows for multiple launches, for the same payload or for different payloads. Second, ideally a reusable rocket has throttling capability, which allows trajectory profiles to be specified and controlled to a greater level of certainty—flight environments not possible with ground

testing. Third, a reusable rocket allows for a returnable test article for inspection and evaluation after exposure to flight environments. The payload test articles can be relaunched to evaluate longer-duration exposure to flight loads.

To achieve the vision, we chose a hybrid rocket motor. The description and schematic of a hybrid rocket motor is illustrated in Figure 2. A hybrid rocket motor was chosen for a variety of reasons:

- **Throttling**—The control of oxidizer flow rate allows for thrust control to better represent a variety of operational missions.
- **Thrust termination and reignition**—Thrust pulsing allows for new trajectory profiles, including a return for landing similar to SpaceX concepts.
- **Safety**—The oxidizer and fuel are kept separate until flight, and if noncryogenic oxidizers are used, then capital overhead is reduced, lowering risks and cost.
- **Performance**—Hybrid rocket performance is acceptable for missions of interest, with specific impulse comparable to that of solids but lower than that of liquids.
- **Cost**—The hybrid rocket fuel and oxidizer options are readily available and affordable and do not require special facilities like liquid and solid rockets do.

To achieve the testing vision, the engineering efforts outlined in Figure 3 gradually build capability, with each step adding a new test resource. The initial steps

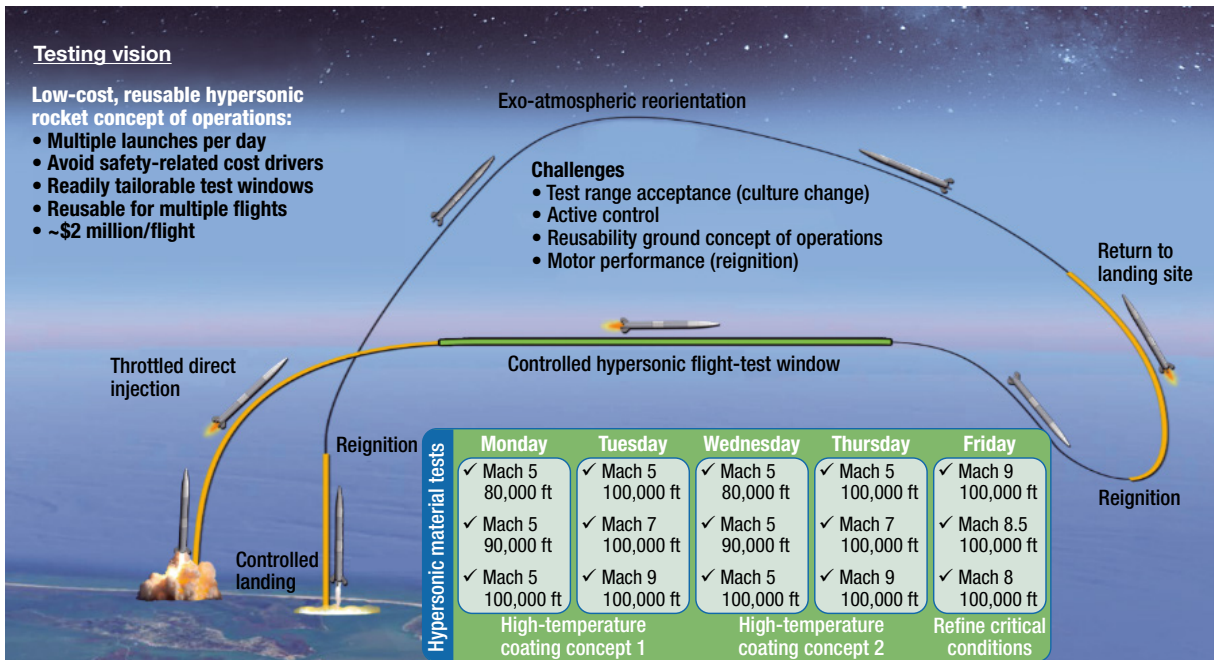


Figure 1. Rapid flight-testing vision. In this vision, a rocket boosts to specific test windows and then returns for landing, which could also be located downrange.

What is a hybrid rocket?

A hybrid rocket uses a solid fuel grain and a liquid or gaseous oxidizer, stored in a tank, which is controlled by a valve through the injector and into the combustion chamber where the fuel grain is stored. Once ignited, the fuel grain starts to pyrolyze and react with the oxidizer to form combustion products, which then exit the nozzle. The motor ignites via a small ignition source and oxidizer passing through the valve. The motor thrust is controlled by the oxidizer flow rate through the valve.

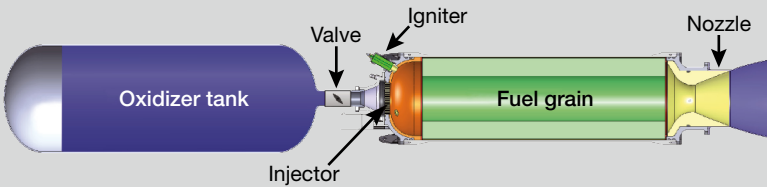


Figure 2. Schematic of a hybrid rocket. (Public domain image courtesy of Jonny Dyer, via Wikipedia, https://commons.wikimedia.org/wiki/File:Hybrids_big-tosvg.svg.)

build ground-test assets to enable exploration testing on hybrid rocket motors while also building infrastructure for future propulsion testing. Next is a subscale rocket capable of low hypersonic conditions to mature the hybrid motor and flight systems while also being a usable asset to flight test technology. Use cases include the following:

- Deploying projectiles to evaluate advanced guidance, navigation, and control
- Sensor terminal flight testing and height of burst testing
- Multi-salvo radar testing
- Defense against hypersonics

Once the subscale rocket is mature, adding another test resource for the nation, the envisioned vehicle development adds additional functionality to support larger

motors, evaluating the enabling technology, and learning to address reusability challenges. Given our vision and a limited budget and schedule, we concentrated on a design for a prototype hybrid engine with a focus on reusability and affordability. The next section of this article describes the design choices made and why and how these choices drove the overall engine design. The second half of the article focuses on the testing, lessons learned, and resulting changes to the engine design. The overall goal is to illustrate how the classic “build a little – test a little” prototyping philosophy can be successfully applied to advance a revolutionary hypersonic testing vision.

APL HYBRID ROCKET DESIGN

In a hybrid propulsion system, one component of the propellant is stored in the solid phase while the other is stored in a liquid or gaseous phase. Most hybrid systems commonly use a liquid oxidizer–solid fuel concept. Figure 4 illustrates the general geometry of a hybrid rocket motor.

In this concept, liquid oxidizer is stored in a tank and pressurized via a gas tank to control the oxidizer upstream pressure and mass flow rate into the combustion chamber.

Oxidizer is injected into a precombustion chamber upstream of the primary fuel grain. The fuel grain contains an axial combustion port with varying geometry that generates fuel vapor to react with the injected oxidizer, which then enters a postcombustion chamber. To improve efficiency, the postcombustion chamber ensures that all fuel and oxidizer are burned before exiting the nozzle. The forward bulkhead includes all the parts in front

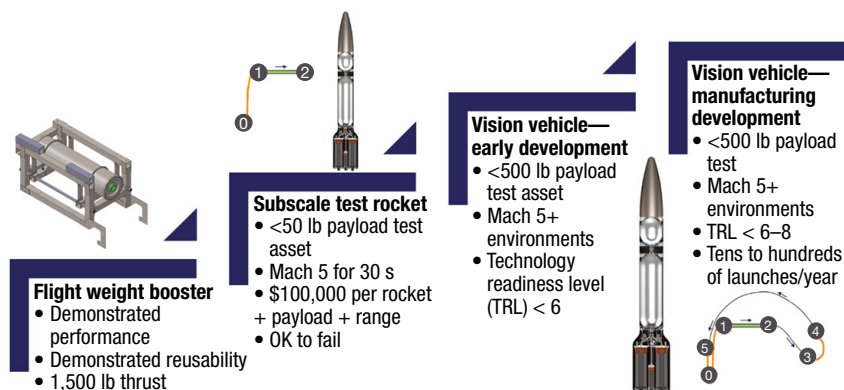


Figure 3. Incremental steps for hybrid rocket development. To achieve the testing vision, the engineering efforts gradually build capability, with each step adding a new test resource. The initial steps build ground-test assets to enable exploration testing on hybrid rocket motors while also building infrastructure for future propulsion testing. Next is a subscale rocket capable of low hypersonic conditions to mature the hybrid motor and flight systems while also being a usable asset to flight test technology.

of the fuel grain (injector and precombustion chamber), while the aft closure assembly contains everything aft of the fuel grain (postcombustion chamber and nozzle housing). All these subcomponents of the chamber are annotated in Figure 4.

To start the design of the rocket motor, first the oxidizer–fuel combination (propellant) has to be chosen. For our design, we chose nitrous oxide (N₂O) and acrylonitrile butadiene styrene (ABS) as the oxidizer–fuel combination. ABS was chosen as the fuel because of its ability to be additively manufactured, enabling rapid development of different fuel grain geometries as a way to increase performance. ABS has sufficient mechanical properties and therefore will not crack or melt in different environments, and it has similar performance characteristics to hydroxyl-terminated polybutadiene (HTPB), which is a widely used fuel for hybrids.²

N₂O was chosen as the oxidizer for this design because of its safety (low toxicity) and its self-pressurizing capability. N₂O at room temperature, 68°F (20°C), has a vapor pressure of approximately 730 psia (5 MPa). With such a high vapor pressure, the self-pressurizing N₂O eliminates the need for additional pressurants or feed systems, which typical hybrid rockets require,³ making N₂O a desirable choice as the oxidizer. However, one of the disadvantages of N₂O is its reduced performance, compared with other oxidizers, since two-thirds of N₂O is nitrogen and nitrogen acts as a diluent, reducing the flame temperature.

After the propellant is selected, the thrust level had to be determined. We chose 400 lbf of thrust because this level gave us the ability to make manageable changes given the available monetary budget. With the propellant and desired thrust levels chosen, we calculated additional performance details to design the fuel grain geometry, oxidizer mass flow rate, nozzle throat, injector, and pre- and postcombustion chamber geometry.

After the propellant was selected, the initial specific impulse (I_{sp}) and oxidizer-to-fuel ratio (O/F) was determined. We performed chemical equilibrium calculations using a NASA computer program, Chemical

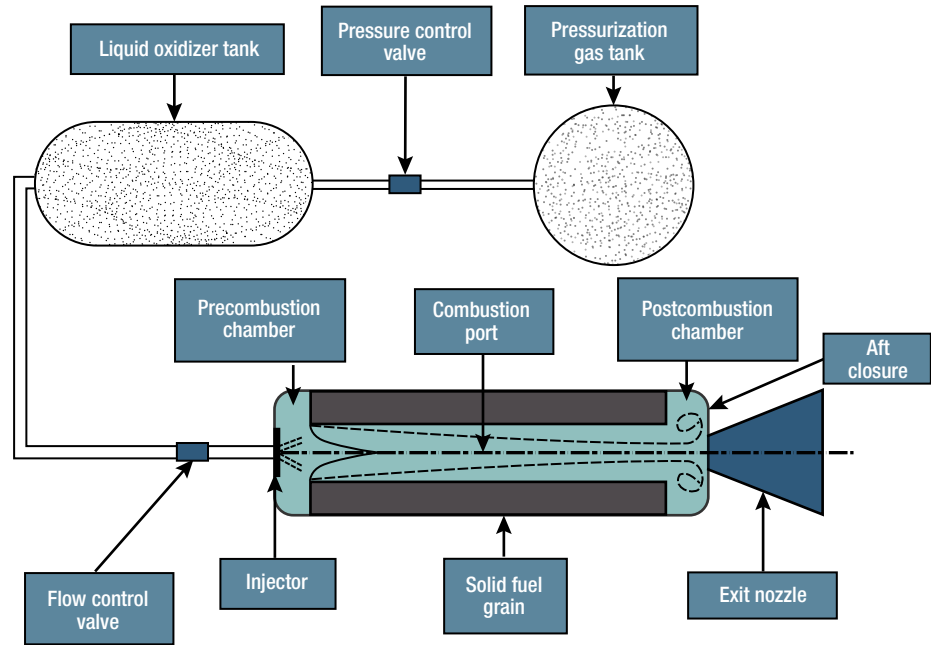


Figure 4. Hybrid rocket motor geometry. In this concept, liquid oxidizer is stored in a tank and pressurized via a gas tank to control the oxidizer upstream pressure and mass flow rate into the combustion chamber. Oxidizer is injected into a precombustion chamber upstream of the primary fuel grain. The fuel grain contains an axial combustion port with varying geometry that generates fuel vapor to react with the injected oxidizer, which then enters a postcombustion chamber. (From Uddanti,⁴ CC BY-NC-ND, <https://creativecommons.org/licenses/by-nc-nd/4.0/>.)

Equilibrium with Applications 2 (CEA2), to identify the theoretical sea-level I_{sp} , optimal O/F, and characteristic velocity (c^*). Equilibrium combustion for a rocket problem using N₂O and ABS as the oxidizer and fuel was assumed. N₂O was chosen from the NASA CEA2 thermodynamic data library,⁵ while the ABS composition was manually entered using the information in Table 1.

Table 1. Input fuel properties for NASA CEA2 code

Fuel	Formula	Molecular Weight (kg/kmol)	Density (kg/m ³)	Heat of Formation (kJ/mol)
ABS	C _{3.85} H _{4.85} N _{0.43}	57.1	975	62.6

Source: Whitmore, Peterson, and Eilers.⁶

Next, the theoretical I_{sp} curve shown in Figure 5 was used in determining the target operating average O/F. The optimal O/F ratio was determined by identifying at what O/F ratio the peak I_{sp} occurs. From this figure, ABS/N₂O has a peak I_{sp} at an O/F ratio of 5.8. The results from the CEA calculations for the optimal O/F were then used to size the rocket motor for a thrust of 400 lbf. First the total propellant mass flow rate was determined by Eq. 1,

$$\dot{m}_{prop} = \frac{I_{sp}}{F}, \quad (1)$$

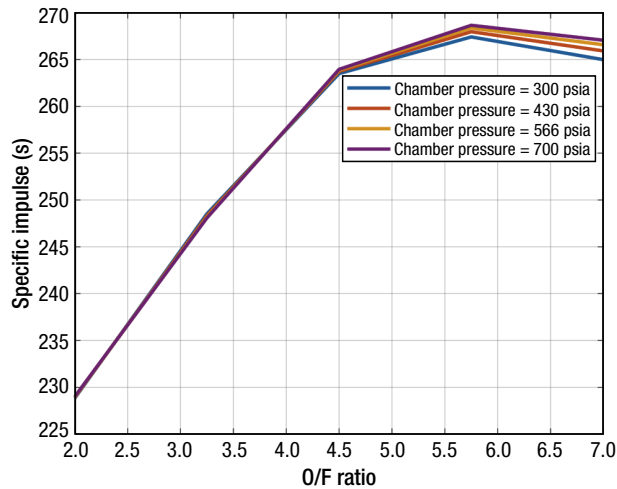


Figure 5. Specific impulse vs. O/F ratios for nitrous oxide and ABS. This figure shows that ABS/N₂O has a peak I_{sp} at an O/F ratio of 5.8.

where \dot{m}_{prop} is the propellant mass flow rate, I_{sp} is the specific impulse (for the 400-lbf motor at sea level), and F is the thrust.

Then, the total mass flow rate of the fuel and mass flow rate of the oxidizer were calculated from the optimal O/F using Eqs. 2 and 3. The mass flow rate of the fuel is \dot{m}_{fuel} and the mass flow rate of the oxidizer is \dot{m}_{ox} . These values are used to size the oxidizer plumbing and the fuel grain geometry. These sizing dimensions are listed in Table 2 (see Humble, Henry, and Larson⁷):

$$\dot{m}_{fuel} = \frac{\dot{m}_{prop}}{1 + \frac{F}{g_0}} \quad (2)$$

$$\dot{m}_{ox} = \dot{m}_{prop} - \dot{m}_{fuel} \quad (3)$$

Using the oxidizer flow rate and the fuel geometry, we used a hybrid rocket motor ballistics code⁸ to size the nozzle throat and calculate the performance for pre- and post-test predictions. The ballistics code produces time-dependent thrust, chamber pressure, and O/F. Time-dependent O/F values are needed because the O/F ratio of a hybrid will vary during the course of the burn.

Oxidizer System

The calculated \dot{m}_{ox} was 2 lbm/s to achieve the required 400 lbf of thrust. This oxidizer mass flow rate was then used in sizing the oxidizer plumbing. Based

Table 2. Fuel grain and nozzle geometry for an initial 400 lbf thrust

Parameter	Value (in.)
Nozzle throat diameter	1
Nozzle exit diameter	2.7
Grain outer diameter	5.75
Grain inner diameter	4
Grain length	20

on the required flow rate, a plumbing code that uses Bernoulli's principle aided in the design of the oxidizer system, which includes loss coefficients for each of the fittings. Figure 6 displays the piping and instrumentation diagram (P&ID). Numerous fittings are needed for instrumentation and safety. A $\frac{3}{4}$ -in. line was required to deliver the oxidizer flow rate while ensuring that the velocity in the pipe stayed below 50 ft/s, per the guidelines from the Compressed Gas Association. We chose the Nitrous Express Lightning 375 solenoid valve (V1 and V2 in Figure 6) for the N₂O valves because of its availability, low cost, and most important, its ability to pulse modulate the oxidizer flow into the chamber. Two N₂O tanks and two 375 solenoid valves were required to obtain the 2 lbm/s of oxidizer flow rate because of the limiting orifice on the tank and valve. Using two oxidizer tanks allowed for longer run times but also helped avoid nitrous expansion upstream of the solenoids because the total pipe diameter increased after the single-run tank line was split into the two solenoid lines. A single solenoid valve is capable of controlling the nitrous flow rate with pulses actuating at 25%, 50%, 75%, and 100% duty cycles. Having two solenoid valves upstream of the injector allows duty cycles from 0% to 100% at 12.5% intervals and a total measured mass flow rate of 1.9 lbm/s, corresponding to 100% duty cycle.

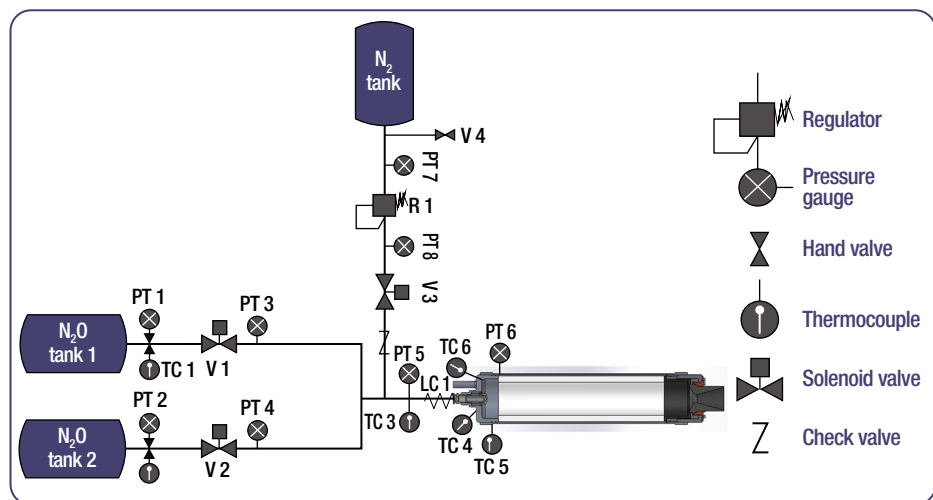


Figure 6. P&ID of oxidizer plumbing. Numerous fittings are needed for instrumentation and safety. See Table 3 for specifications of the measurement devices used.

A tee was used to combine the nitrous oxide after the two solenoid valves, where it then entered the injector before entering the combustion chamber, as shown in the P&ID. A nitrogen purge system extinguished combustion upon completion of a test event.

Nozzle Geometry

When calculating the nozzle throat area, three key assumptions include required chamber pressure, c^* , and the total mass flow rate ($\dot{m}_{ox} + \dot{m}_{fuel}$), where the regression rate correlation is what dictates the \dot{m}_{fuel} . The desired chamber pressure was 400 psia. We used the regression rate multiplier and exponent described by Nardozzo, Popkin, and Smith⁸ because in this study they used the same propellant, resulting in the nozzle geometry characteristics listed in Table 2.

Injector

The oxidizer injection characteristics play a substantial role in hybrid rocket motor performance. In APL's configuration, a two-phase oxidizer (N_2O) is injected into the combustion chamber by means of an atomizer (injector), and a spray is formed. The liquid oxidizer droplets are vaporized in the precombustion chamber via the injector, and heat feedback from the flame flows through the combustion port and then reacts with the fuel grain to achieve stable combustion. The injector determines the mass flow rate into the combustion chamber,⁹ while the combustion process is primarily influenced by the incoming oxidizer flow pattern. Furthermore, the flow characteristics can significantly affect the overall behavior of the motor in terms of thrust, fuel consumption, combustion efficiency, and combustion stability. The APL design initially used a commercial off-the-shelf spray injector from BETE, model SS12, as shown in Figure 7.¹⁰ This injector features 12 ports that are angled at 35° from the centerline of the motor. This injector was chosen because it reliably produces choked flow, which prevents known issues with feed-coupling instabilities,¹¹ and has enough discharge area to deliver the mass flow rate required for the system pressures (i.e., line pressure and chamber pressure).

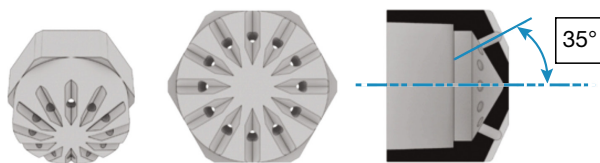


Figure 7. Images of the BETE SS12 injector. This injector features 12 ports that are angled at 35° from the centerline of the motor. This injector was chosen because it reliably produces choked flow, which prevents known issues with feed-coupling instabilities and has enough discharge area to deliver the mass flow rate required for the system pressures (i.e., line pressure and chamber pressure).



Figure 8. Forward-facing step in a hybrid rocket motor. The forward-facing step of the fuel grain promotes favorable gasification of the oxidizer for stable combustion and improved combustion efficiency.

Precombustion and Postcombustion Chamber

We then chose the pre- and postcombustion chamber dimensions around the fuel grain design. American Rocket Company (AMROC) testing found that precombustion chambers are important for liquid oxidizer injection because they allow for the expanded N_2O to adequately atomize before reacting with the flame front,^{12,13} thereby resulting in stable combustion and reducing the probability of a flame-holding instability (this instability is described later in the article). The forward-facing step of the fuel grain, shown in both Figure 4 and Figure 8, promotes favorable gasification of the oxidizer for stable combustion and improved combustion efficiency.¹⁴ AMROC found that a forward-facing step sized at 13% of the full motor diameter increased residence time of the oxidizer to suppress acoustic instabilities (described in the next section).¹⁵ The original APL design had a 14% forward-facing step, which is comparable to the AMROC recommendation.

The precombustion chamber length was then set to have a length-to-diameter ratio, referenced on the outer diameter of the fuel grain, of 0.4, fixing the precombustion chamber length to 2-in., per Humble, Henry, and Larson.⁷ Once the oxidizer atomizes in the precombustion chamber, a boundary layer grows along the inner surface of the fuel grain where the flame forms inside the boundary layer. If the gasified propellants were exhausted right after reaching the end of the fuel grain, the rocket motor would not perform as well, since the residence time for those gases within the motor would not be long enough for complete combustion. Therefore, a postcombustion chamber is used to increase the residence time and promote mixing to ensure complete combustion and increase efficiency. Typically, the postcombustion chamber has an L/D of 0.5 to 1. This hybrid design uses an L/D of 0.6, which results in a postcombustion chamber length of 2.895-in. (see Humble, Henry, and Larson⁷).

INSTABILITY AND REUSABILITY CONSIDERATIONS

During the design process, the fuel grain and chamber were sized to achieve the required performance; however, reusability needs to be considered too. The

two main challenges that needed to be accounted for in the design were the combustion instabilities and thermal management of the various motor components. This section discusses in more detail both of these challenges, and how they were addressed and/or mitigated in the design.

Combustion Instabilities

Overall, the hybrid combustion process tends to produce more oscillatory pressure versus time characteristics than either liquid or solid rocket engines. However, a well-designed hybrid typically limits combustion noise to approximately 2% to 3% of mean chamber pressure. When pressure oscillations occur in hybrid motors, they are observed to grow to a limiting amplitude dependent on such factors as the oxidizer feed system and injector characteristics, oxidizer mass velocity, fuel grain geometric characteristics, and mean chamber pressure level. Hybrid motors have exhibited two basic types of instabilities in static test environments: an instability induced by the oxidizer feed system (nonacoustic) and a flame-holding instability (acoustic). Instability of the oxidizer feed system is essentially a “chugging” type characteristic, illustrated in Figure 9, and arises when the feed system is sufficiently “soft.” In terms of this system, soft implies a high level of compression from two-phase flow in the oxidizer feed lines combined with insufficient isolation from the motor combustion process. To counteract this chugging-type instability, the motor’s feed/injection system was stiffened by increasing the injector pressure drop (making propagation of motor pressure disturbances upstream through the feed system more difficult) and eliminating sources of compressibility in the feed system.¹⁴ This was done by ensuring that the injector pressure drop was 40% of the chamber pressure.⁷ Flame-holding instabilities are the second

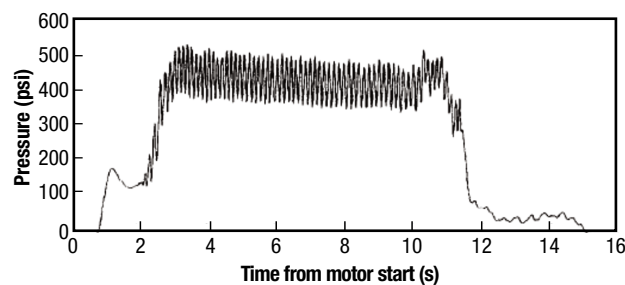


Figure 9. “Chugging” type characteristic. Periodic, large-amplitude, low-frequency combustion pressure oscillations are an example of oxidizer feed system combustion instability also known as a chugging-type instability. Hybrids typically observe combustion noise on the order of 2% to 3% of mean chamber pressure; however, noise rising above 2% to 3%, as shown in this figure, signifies a combustion instability. This chugging-type instability is an issue and in some cases can cause a motor failure. (Reprinted from Sutton and Biblarz,¹⁴ with permission.)

type of instability a hybrid motor faces and arise because of inadequate flame stabilization in the boundary layer; they are not associated with the oxidizer feed system flow perturbations.

Thermal Management

Thermal management had to be addressed for three parts: the precombustion chamber, the postcombustion chamber, and the nozzle. Thermal management is an important part of this design to ensure that the rocket motor can withstand the high temperatures for a test window of 30–60 s. While the focus of the hybrid motor design was reusability, we understood that not all parts of the motor were going to be reusable and would probably need to be replaced between motor tests.

For other hybrid motor designs, the precombustion chamber section was insulated using paper phenolic; thus, the same insulation was chosen for the design of the APL hybrid motor.^{16,17} One of the main concerns was the postcombustion chamber, where the hot combustion gases reside to increase motor efficiency. The temperature within this area is on the order of 5,792°F (3,200°C); therefore, the postcombustion chamber needed to survive this high-temperature environment while at the same time remaining reusable. To manage this environment, a postcombustion chamber insert was conceived and designed for easy replacement after each test. The aft closure design is shown in Figure 10. Here, the postcombustion chamber insert is made up of the ethylene propylene diene monomer (EPDM) insulation, which is glued into a 3-D-printed ABS closure. This ABS closure screws into the metal closure, which houses the postcombustion chamber and nozzle. The nozzle is then held in place by a retention ring and bolts. This design allows for easy replacement of the

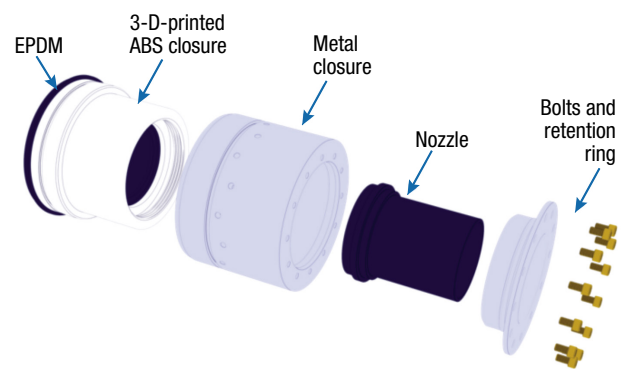


Figure 10. Aft closure assembly. The postcombustion chamber insert is made up of the EPDM insulation, which is glued into a 3-D-printed ABS closure. This ABS closure screws into the metal closure, which houses the postcombustion chamber and nozzle. The nozzle is then held in place by a retention ring and bolts. This design allows for easy replacement of the postcombustion chamber insert between tests while all other parts remain reusable.

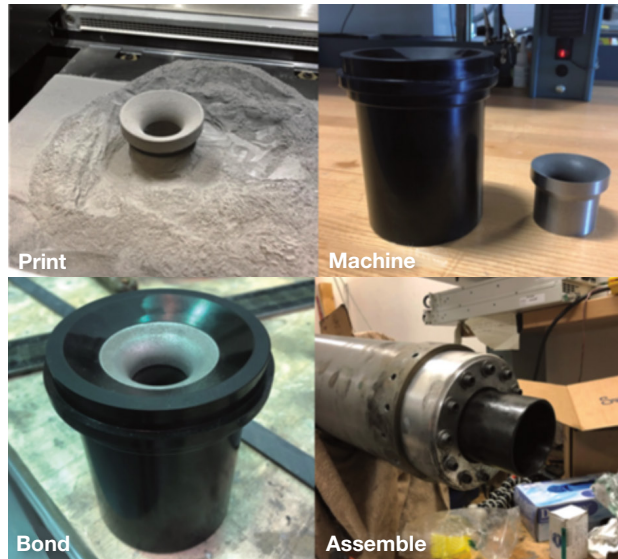


Figure 11. Tungsten throat insert for a reusable rocket nozzle.

postcombustion chamber insert between tests while all other parts remain reusable.

We first chose a commercial off-the-shelf glass phenolic nozzle, from Rocket Motor Components, with a throat diameter of 1 in. This nozzle was purchased because it is readily available and low cost; however, we understood that it would erode. As the nozzle erodes, the chamber pressure within the motor is reduced. Therefore, during the test campaign we used other reusable nozzle designs, such as a non-eroding tungsten throat insert (see Figure 11). The APL hybrid rocket motor design is shown in Figure 12.

The APL motor was designed to be modular to allow for flexibility in the lengths of the fuel grain and the pre- and postcombustion chambers, which are easily

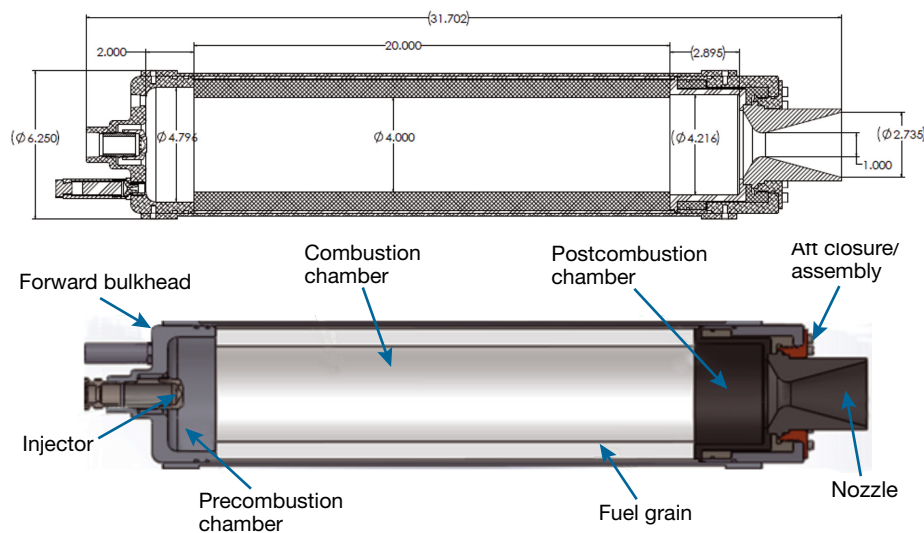


Figure 12. APL hybrid rocket motor combustion chamber design. Dimensions (top) and nomenclature (bottom) are noted.

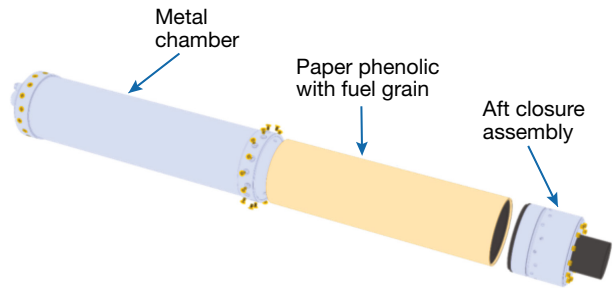


Figure 13. Schematic of the rapid assembly and disassembly of combustion chamber. The fuel grain is replaced by unscrewing the aft closure assembly and pulling out the burned paper phenolic/fuel grain insert and then replacing it with a new insert.

disassembled and reassembled for a rapid turnaround with multiple tests in a single day. The fuel grain is replaced by unscrewing the aft closure assembly and pulling out the burned paper phenolic/fuel grain insert and then replacing it with a new insert, as illustrated in Figure 13. The postcombustion chamber insert is also replaced, and the aft closure component is reassembled and reattached for the next motor firing.

GROUND-TEST FACILITY AND EXPERIMENTAL SETUP

The hybrid rocket test facility located on the APL campus consists of an isolated instrumentation building and nearby outdoor enclosure. The hybrid rocket testing occurs in the outdoor enclosure, while personnel shelter in the instrumentation building, which is a safe distance away, to conduct test events. Figure 14 shows the inside of the outdoor enclosure. Shown in the background are the two oxidizer tanks (known as run tanks), each connected to a Nitrous Express Lightning pulse-actuated solenoid valve and the hybrid motor combustion chamber resting on the thrust stand. Figure 6 shows the P&ID schematic of this setup, which complements Figure 14 in conveying the overall setup and operation of the APL hybrid rocket motor.

The igniter assembly for the motor included a stainless steel housing with a PAVE Technology 2064 hermetic electric feedthrough to pass in 12-V, 3-A current to initiate an Aerotech D13-7W solid motor. The observed

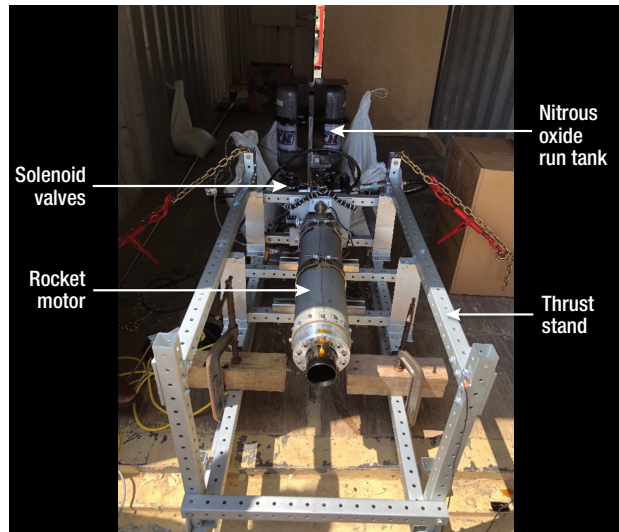


Figure 14. APL hybrid rocket testing facility with test stand and oxidizer run tanks depicted. Along with Figure 6, which shows the P&ID schematic drawing of this setup, this image conveys the overall setup and operation of the APL hybrid rocket motor.

time from the ignition command to the start of the Aerotech motor is approximately 0.5 s. After the motor starts, hot combustion products are ejected into the precombustion chamber during the nominal burn time of 1.5 s. Approximately 1 s after the Aerotech motor starts, the oxidizer is introduced. First, a single solenoid is opened at 50% duty cycle and then, after 0.33 s, the second solenoid is opened at 50% duty cycle. After another 0.33 s, both solenoids are operated at 75% duty cycle. Finally, after another 0.33 s, both solenoid valves are opened to 100% for a total of 1.9 lbm/s flow rate. Figure 15 shows the solenoid and igniter command signals leading to ignition and combustion. This process has proven to provide reliable ignition as long as the igniter wire successfully ignites the Aerotech motor. The controller for the ignition sequence and entire test event is driven by an Arduino controller.

During the test, data acquisition includes multiple pressure and temperature sensors in addition to a load cell to monitor the motor thrust during each test. Table 3

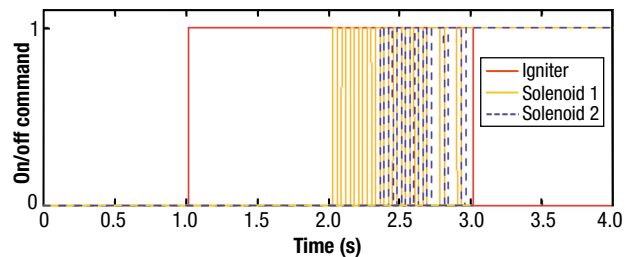


Figure 15. Time trace of solenoid and igniter commands leading to maximum flow rate combustion. This process has proven to provide reliable ignition as long as the igniter wire successfully ignites the motor.

Table 3. Specifications of measurement devices used

Measurement Device	Company/ Model No.	Corresponding No. in Figure 6
Temperature	Omega/TC-K-NPT-E-72	TC 1, 2, 3
Temperature	Omega/SA1-K-SRTC	TC 4, 5, 6
Pressure transducers	Setra/206	PT 1, 2, 3, 4, 5, 6
Load cell	Omega/LC305	LC 1

lists the instrumentation used during the tests, while Figure 6 shows the locations of each pressure, temperature, and thrust sensor used. The pressure sensors are placed such that they measure each of the nitrous bottle pressures, nitrous pressure upstream and downstream of the solenoids, and the chamber pressure. The thermocouple (type K) locations vary based on the objective of the test, but there is typically a thermocouple on the forward bulkhead, on the neck of the injector, on the exterior of the motor case opposite the precombustion chamber, and on the exterior of the motor case near the postcombustion chamber.

TEST RESULTS/IDENTIFICATION OF A THERMAL MANAGEMENT ISSUE

We conducted a test campaign, after manufacturing and assembling the designed 400-lbf rocket motor, to evaluate the motor's performance and validate the ballistics model. The test duration was set to 6 s, with a 1-s start-up sequence to ensure proper ignition. We chose the start-up transient of 1 s so that enough heat from the igniter would start to pyrolyze the fuel grain while also slowly introducing the oxidizer to ensure the flame would not be blown out. We chose a duration of 6 s for

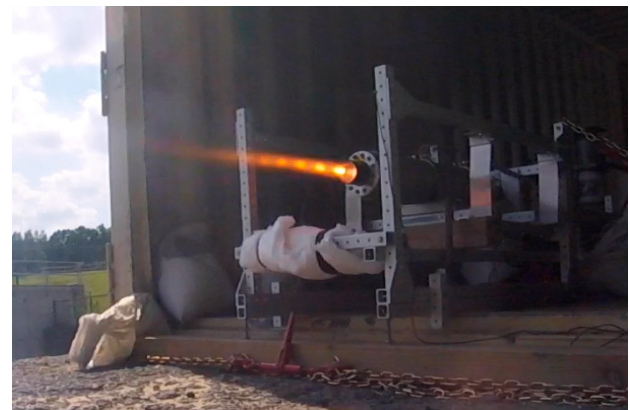


Figure 16. Still image of the first 6-s test. This test campaign evaluated the motor's performance and validated the ballistics model. The test duration was set to 6 s, with a 1-s start-up sequence to ensure proper ignition. We chose the start-up transient of 1 s so that enough heat from the igniter would start to pyrolyze the fuel grain while also slowly introducing the oxidizer to ensure the flame would not be blown out.

the test campaign to meet our test objectives of reaching steady state for a minimum of 5 s. This duration was long enough to ensure that there were sufficient data to obtain the performance parameters that were needed and short enough to allow observation of whether the motor experienced any heating. Figure 16 is an image of the hybrid motor operating during the start-up transient of the test.

Figure 17 shows all signals and pressure and thrust measurements recorded during the run. The difference between the nitrous tank and solenoid input pressure measurements shows that the pressure drop over the length of plumbing averaged 30 psid. This pressure drop over the length of the plumbing is less than what the plumbing code predicted and is a positive result in terms of the overall system. Loss coefficients were taken from fluid textbooks and are most likely higher than what was observed. The thin black curve shows the pressure downstream of the solenoid valves after the flow from each run tank merges. The pressure difference between the blue and black curves shows an average pressure drop across

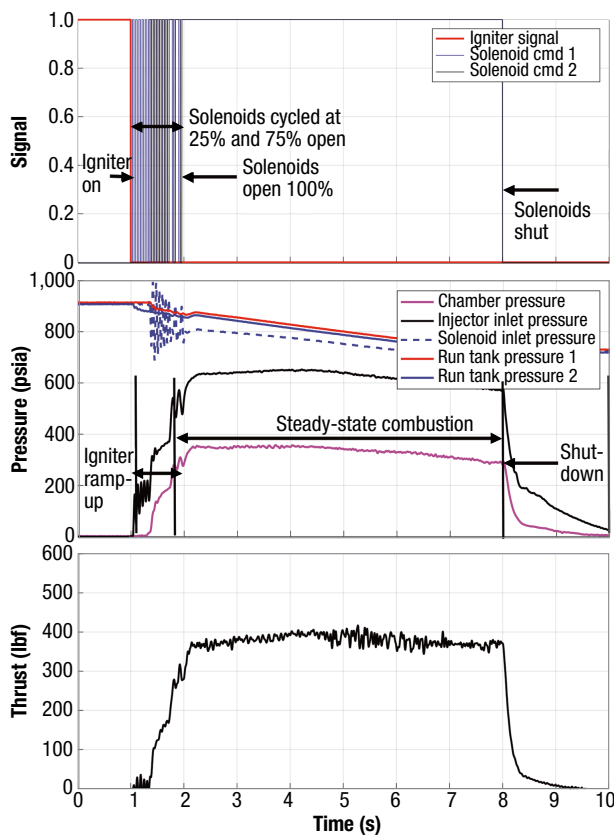


Figure 17. Test 1 data including signals (top), pressures (middle), and thrust (bottom). In the middle panel, the thin black curve shows the pressure downstream of the solenoid valves after the flow from each run tank merges. The pressure difference between the blue and black curves shows an average pressure drop across the solenoids near 100 psid. Finally, the magenta curve shows the chamber pressure during the run.

the solenoids near 100 psid. Finally, the magenta curve shows the chamber pressure during the run. All pressure readings show fairly consistent pressure drops across the system for the duration of the run. Another interesting observation is that when the chamber pressure measurements during the initiation sequence showed the lowest throttle of 25% (one solenoid at 50%), thrust was produced, thereby demonstrating an indication of throttled performance. Also, the ignition rise time is quantified from the start of the igniter going off to 75% max chamber pressure, as annotated in the figure.

Figure 17 shows the thrust profile during the start-up sequence, the 6-s thrust duration, and the shutdown sequence of the test. The thrust profile tracks well with the chamber pressure; however, during the last 3 s of the burn, the chamber pressure starts decreasing while the thrust remains constant, indicating nozzle erosion based on Eq. 4. The nozzle throat was measured after the test and an erosion rate of 8 mils/s was calculated using the test data,

$$F = P_c A_t C_f \tag{4}$$

where P_c represents the chamber pressure, A_t is the nozzle throat area, and C_f is the thrust coefficient.

Rearranging this equation for A_t , as shown in Eq. 5, reveals that if the thrust stays constant with decreasing pressure, the nozzle throat area must increase, since C_f stays fairly constant:

$$A_t = \frac{F}{P_c C_f} \tag{5}$$

Also note that thrust measured during the start-up sequence is consistent with the combustion chamber pressure measurements shown in Figure 17 and the solenoid cycling introduced pressure fluctuations at the solenoid inlet.

Immediately following this first test, the combustion chamber was disassembled for post-test inspection. The only anomalous observation from this test was the

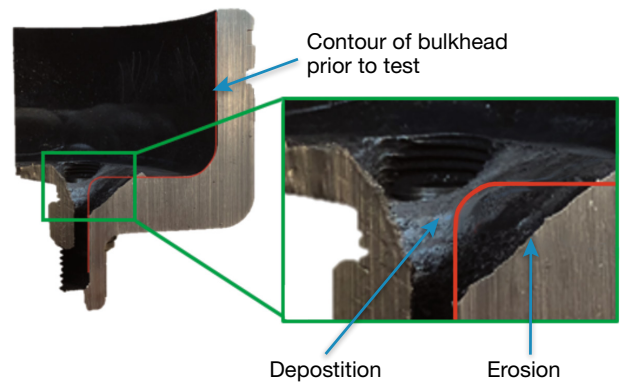


Figure 18. Post-test sectioned forward bulkhead. This figure shows the change to the original inner contour (shown by the red curve) due to high-temperature flow near the injector.

eroded forward bulkhead in the vicinity of the injector (shown in Figure 18). The red curve in Figure 18 illustrates the original forward bulkhead contour before the test. Both erosion and deposition of the aluminum are evident in this image. Without management of this thermal environment, the combustion chamber would probably not be able to operate for much more than 6 s and would not be reusable. Forward bulkhead thermal performance was considered when selecting the material, but empirical thermal environment proved to be higher than expected. The forward bulkhead was fabricated from aluminum 6061. Once it reaches 212°F, aluminum 6061 starts losing its mechanical strength by 10%; it loses as much as 50% at 392°F, and it starts melting at 1,090°F.¹⁸ The forward bulkhead saw temperatures exceeding 1,090°F, which significantly reduced the mechanical strength (up to 75% reduction on yield strength), ensuring that this motor design would not last for much longer than 6 s. As designed, the thermal load on the forward bulkhead is unacceptable for a reusable hybrid rocket motor. This motivated a redesign of the APL hybrid rocket motor. The following section discusses the redesign and additional testing needed to verify it.

REDESIGN CAMPAIGN

As previously discussed, APL had embarked on a test campaign to evaluate the performance of a hybrid rocket motor design. However, once the thermal management issue was discovered from the initial test, focus shifted to solving the heating problem at the forward bulkhead. In the interest of efficiently and quickly exploring the problem, we used an unsystematic test approach and often changed multiple design elements at once based on intuition, test results, and literature research. We made these choices to best manage the funding and schedule limitations of the program.

Four tests were conducted to investigate the effect of design changes on forward bulkhead heating. Leveraging the observations from other researchers, the evolution of the forward bulkhead design involved changes to both the precombustion chamber (length) and the injector (spray angle and individual port contours). The following section discusses the original combustion chamber design and details the iterations and discoveries toward a successful design that achieves a reusable forward bulkhead.

The thermal heating result from the first test was unexpected because the precombustion chamber design was similar to other documented chambers,^{19–21} and the N_2O expands just after the injector, resulting in a very cold ($\sim 5^\circ F$) gas in the precombustion chamber. However, other researchers also found precombustion thermal management problems^{22,23} where post-test observations showed a damaged injector. In these cases, they

changed the injector from aluminum to stainless steel to withstand the heating²² or increased the length of the precombustion chamber.²³ In addition, Jones, Myre, and Cowart found that the fluid motion resulting from a swirl injector provides a thermal barrier via the oxidizer between the flame front and the forward bulkhead, whereas the fluid motion resulting from conical axial injectors does not.²⁴

Figure 19 shows the primary flow features associated with a conical, axial-injection hybrid rocket similar to the design tested at APL. This figure shows regions of recirculation that are potentially responsible for introducing hot gases at the injector from the flame front at the forward end of the fuel grain.

In view of other researchers experiencing precombustion chamber overheating, we conducted a SOLIDWORKS Flow Simulation analysis of the N_2O flow behavior in the forward bulkhead area. The analysis showed a center recirculation driving flow back into the injector area of the forward bulkhead, as illustrated in Figure 20, where the oxidizer transports significant heat to the forward bulkhead.

More than 50% of the recirculation occurred over the flame front, and we decided that the heat input from the flame to the nitrous oxide was the primary contributor to the forward bulkhead heating. We also postulated that the 35° injector spray angle was contributing to the recirculation region and could possibly pose a future problem with combustion instability. Therefore, test 2 used a custom, pure axial injector design with straight ports and the same orifice diameters as the BETE injector displayed in Figure 21.

Furthermore, based on the literature, we redesigned the precombustion chamber as well. The precombustion

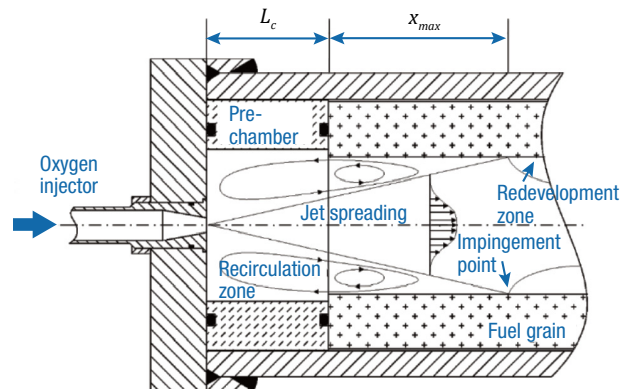


Figure 19. Schematic of a conical axial-injection hybrid rocket with the main flow characteristics downstream of the injector and in the precombustion chamber. The design shown is similar to the one tested at APL, and the figure shows regions of recirculation that are potentially responsible for introducing hot gases at the injector from the flame front at the forward end of the fuel grain. (From Carmicino and Sorge,¹³ reprinted by permission of the American Institute of Aeronautics and Astronautics, Inc.)

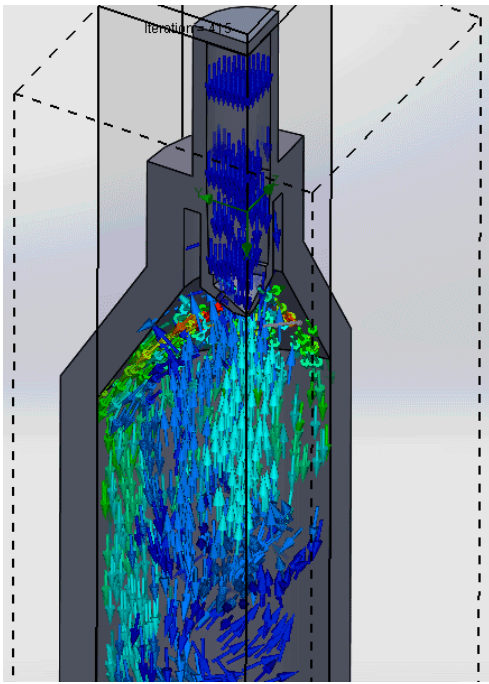


Figure 20. Flow recirculation of nitrous oxide. The analysis showed a center recirculation driving flow back into the injector area of the forward bulkhead, where the oxidizer transports significant heat to the forward bulkhead.

chamber was lengthened from $L_c = 2$ in. to $L_c = 4.8$ in. (where L_c is in reference to Figure 19) to obtain a pre-combustion chamber length-to-diameter ratio of one based on the upper limit from Humble, Henry, and Larson⁷ and Gomes, Rocco, and Rocco²³ in an effort to reduce the heat feedback from the flame to the forward bulkhead. As the length of the precombustion chamber is increased, the temperature will gradually decrease due to reduced heat transfer to the walls.²⁵ Other than the length change, the precombustion chamber geometry stayed the same.

Figure 22 shows the pressure measurements of the newly designed precombustion chamber and injector, which demonstrates a strong feed-coupling instability, as indicated by the highly oscillatory pressure signal in both the combustion chamber and inlet to

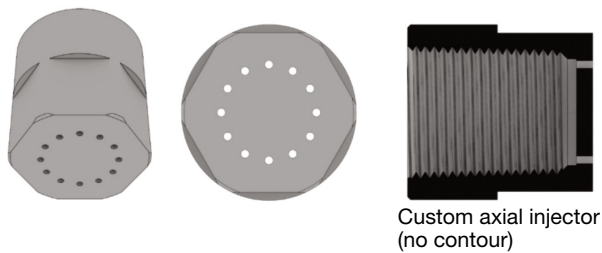


Figure 21. Custom axial injector design. Test 2 used a custom, pure axial injector design with straight ports and the same orifice diameters as the BETE injector.

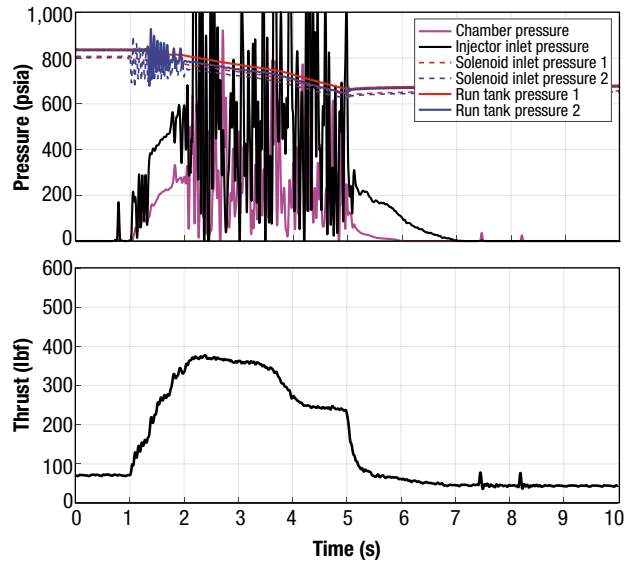


Figure 22. Test 2 data including pressure and thrust measurements. The newly designed precombustion chamber and injector demonstrated a strong feed-coupling instability, as indicated by the highly oscillatory pressure signal in both the combustion chamber and inlet to the injector. The initial thrust in test 2 was slightly lower than in the first test because the fuel surface area had to be reduced to achieve the increased precombustion chamber length. Test duration was also decreased from 6 s to 4 s as a result of the heating issues observed during test 1.

the injector. This was due to the injector ports being simple flat plate orifices such that the nitrous oxide was not choked across the injector. As discussed previously, hybrids need a 40% pressure drop across the injector (from in front of the injector to the combustion chamber) to ensure that the flow is choked. This was not the case for this test. The injector inlet pressure was equal to or below the chamber pressure at 2.2 s in Figure 22. However, since N_2O is a two-phase liquid, the design approach of an injector changes based on the vapor pressure of the liquid, and this was remedied by re-designing the injector with longer contoured ports based on Waxman.²⁶ Waxman thoroughly discusses injector design to achieve ideal N_2O injection and safe hybrid motor operation (i.e., no feed-coupling instabilities). Based on his work, we designed a new custom injector with a chamfered inlet and L/D ratio of 12 on the throat that expanded at a 1.5° half-angle to the chamber, as shown in Figure 23. This would ensure that the injector acted as a cavitating injector, forcing the N_2O to cavitate inside the diverging portion of the injector to sufficiently isolate the oxidizer plumbing from the chamber at varying system pressures.

Figure 22 shows the thrust measured for the second test. The initial thrust was slightly lower than in the first test because the fuel surface area had to be reduced to achieve the increased precombustion chamber length; in this test, the fuel grain length was reduced by 2.8 in.

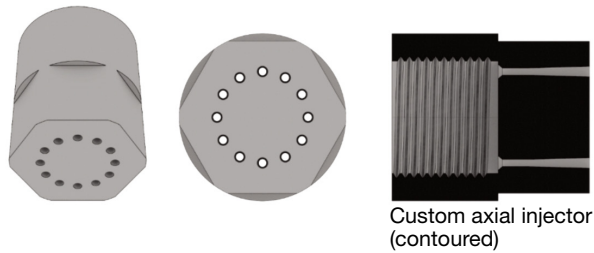


Figure 23. Custom axial injector with contoured ports. Based on Waxman's work,²⁴ we designed a new custom injector with a chamfered inlet and L/D ratio of 12 on the throat that expanded at a 1.5° half-angle to the chamber. This design ensured that the injector acted as a cavitating injector, forcing the N₂O to cavitate inside the diverging portion of the injector to sufficiently isolate the oxidizer plumbing from the chamber at varying system pressures.

However, the thrust also drops after 2 s. This drop is due to the feed-coupling instability reducing the nitrous flow rate, which in turn reduces the thrust.

Despite the instability, this test demonstrated a successful reduction in heating on several areas of the forward bulkhead, as no melting was observed. The time history of the thermocouple data is plotted in Figure 24. Note that the temperature continues to rise at the conclusion of the test at 5 s. This is due to a thermal lag in the temperature response because the internal heat takes a finite amount of time to conduct through the bulkhead to the outer surface where the thermocouple is located. Because of the thermal lag, analysis of the data should also consider the rate of change in temperature as a metric evaluation of the reduction of internal heating in the precombustion chamber. The results from this second test support the hypothesis that the recirculation region was initially drawing too much heat from the flame front and the precombustion chamber was not long enough to effectively isolate the high temperature of the flame front from the forward bulkhead, which caused the overheating.

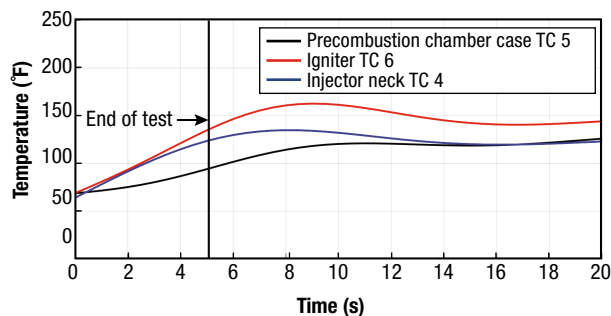


Figure 24. Test 2 time trace of the hybrid motor temperature data. Shown are measurements for the side of the precombustion chamber (black), the forward face of the injector neck (red), and the neck of the injector (blue).

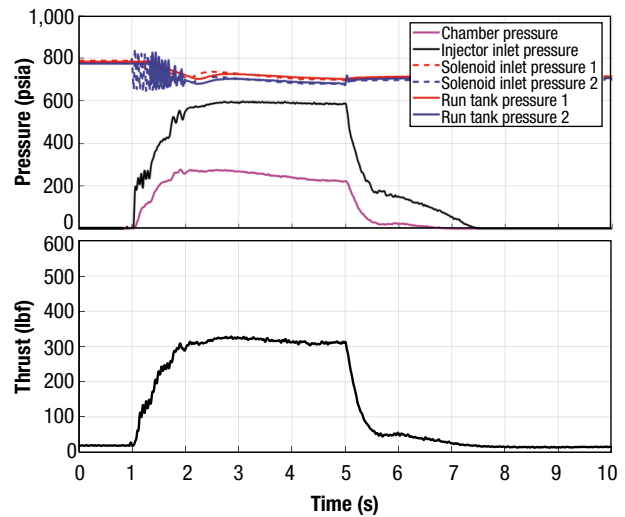


Figure 25. Test 3 data including pressures and thrust. The thrust measured during the third test is comparable to that seen during the second test, yet lower than that of the first test. This thrust reduction was expected because the fuel grain length (reduced by 2.8 in.) and overall surface area were reduced in order to increase the precombustion chamber length.

A third test was conducted, while the new custom axial contoured injector was being designed, to confirm the hypothesis that lengthening the precombustion chamber would reduce the forward bulkhead temperatures. The change for the third test was to eliminate the feed-coupling instability by using the original BETE SS12 injector. Data from this test, plotted in Figure 25, indicate that the feed-coupling instability was eliminated by the lack of large oscillations in the combustion chamber and injector inlet pressure measurements that are shown in Figure 22. Note that the run tank pressures were low compared to the first two tests (800–900 psia), which also result in lower injector inlet and combustion chamber pressures. The run tank pressures have to be considered before every test to ensure they are not low enough to fall below the 40% margin on the N₂O vapor pressure that is needed to eliminate feed-coupling instabilities. For this specific test, the pressure was well above the margin. Figure 25 shows that the thrust measured during the third test is comparable to that seen during the second test, yet lower than that of the first test. This thrust reduction was expected because the fuel grain length (reduced by 2.8 in.) and overall surface area were reduced in order to increase the precombustion chamber length. There are no thermocouple data for the third test because of an electrical short in the thermocouple wires. However, the pressure data for the injector and chamber pressure indicate that the BETE SS12 injector eliminated the feed-coupled instability.

We conducted a fourth and final test with the new custom axial injector with contoured ports. This final

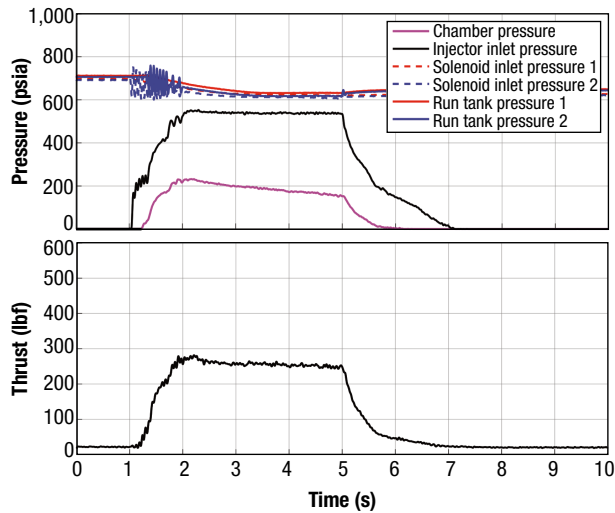


Figure 26. Test 4 data including pressures and thrust. The pressure-time history demonstrates the successful elimination of feed-coupling instability and a corresponding thrust reduction compared to prior tests because of the reduced overall system operating pressures and shortened fuel grain length. Yet, this test had a similar oxidizer mass flow rate as test 3 but a lower thrust value with the same fuel grain geometry. This is an indication that the pure axial injector reduced the regression rate of the fuel grain compared to the conical injector, which was observed in other research.

test verified that a longer precombustion chamber, paired with a custom injector, reduced the heating on the forward bulkhead as desired. The test data in Figures 26 and 27 show evidence of a successful redesign of the APL hybrid motor to address the thermal management of the forward bulkhead. Figure 26 shows the pressure and thrust measurements for the final test. The pressure-time history demonstrates the successful elimination of feed-coupling instability. Further note that the run tank pressures were low again compared to the first three tests, contributing to the lower injector inlet and combustion chamber pressures. Figure 26 shows a corresponding thrust reduction compared to prior tests because of the reduced overall system operating pressures and shortened fuel grain length. Yet, this test had a similar oxidizer mass flow rate as test 3 but a lower thrust value with the same fuel grain geometry. This is an indication that the pure axial injector reduced the regression rate of the fuel grain compared to the conical injector, which was observed in other research.²⁷ The pure axial injector is more suitable in eliminating acoustic instabilities relative to the conical injector¹⁴ because it helps produce a counter-flowing hot gas recirculation zone, similar to that of a rearward-facing step, at the head end of the diffusion flame. This provides sufficient oxidizer preheating at the leading edge of the boundary-layer diffusion flame to stabilize combustion.

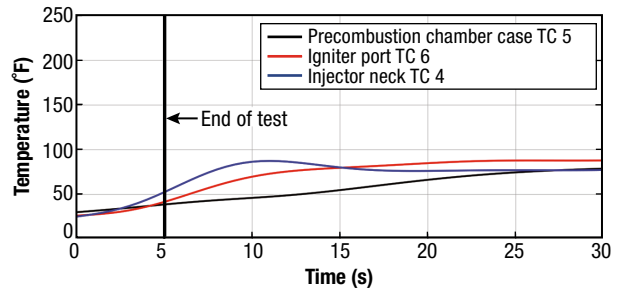


Figure 27. Test 4 time trace of the hybrid motor temperature data. Shown are measurements for the side of the precombustion chamber (black), the forward face of the injector neck (red), and the neck of the injector (blue).

Figure 27 shows the thermocouple data for the final test, illustrating that the temperature of the forward bulkhead is well below the temperature where the mechanical strength of aluminum begins to reduce because of elevated temperature, as previously discussed. The data show that the temperature on the external surface of the forward bulkhead is 86°F (30°C). The Department of Defense handbook¹⁸ notes that the mechanical strength is reduced by 10% when aluminum 6061 reaches 212°F (100°C). Again, note that the temperatures for all thermocouple locations in the final test continued to rise after the conclusion of the test at 5 s—the same as in the second test. However, comparing the rate of change of the temperature (i.e., the slope of the temperature-time history) between the fourth and second tests reveals that the rate for the fourth test is smaller than the rate for the second test, which indicates that the forward bulkhead heating was reduced for the fourth test. The heating rate in the fourth test was reduced by 113% from the second test. These results indicate that the design assessed in the fourth and final test is an improvement over all previous designs, reducing the forward bulkhead heating yet continuing to produce stable combustion.

Table 4 and Figure 28 summarize all four tests and the corresponding critical design features that were changed and evaluated.

Table 4. Summary of tests executed with critical design features evaluated

Test	Dura- tion (s)	Injector	Spray Angle (deg)	Precombus- tion Chamber Length (in.)
1	6	SS12	35	2.0
2	3	Custom axial straight ports	0	4.8
3	3	SS12	35	4.8
4	6	Custom axial with contoured ports	0	4.8

SUMMARY AND CONCLUSIONS

Given our vision and a limited budget and schedule, our focus was to design a prototype hybrid rocket motor with an emphasis on reusability and affordability. This article described the design choices we made, why we made them, and how they drove the overall engine

design. Our choices and decisions illustrate how the classic “build a little – test a little” prototyping philosophy can be successfully applied even to an advanced and revolutionary hypersonic testing vision. We investigated a forward bulkhead overheating issue that threatened the

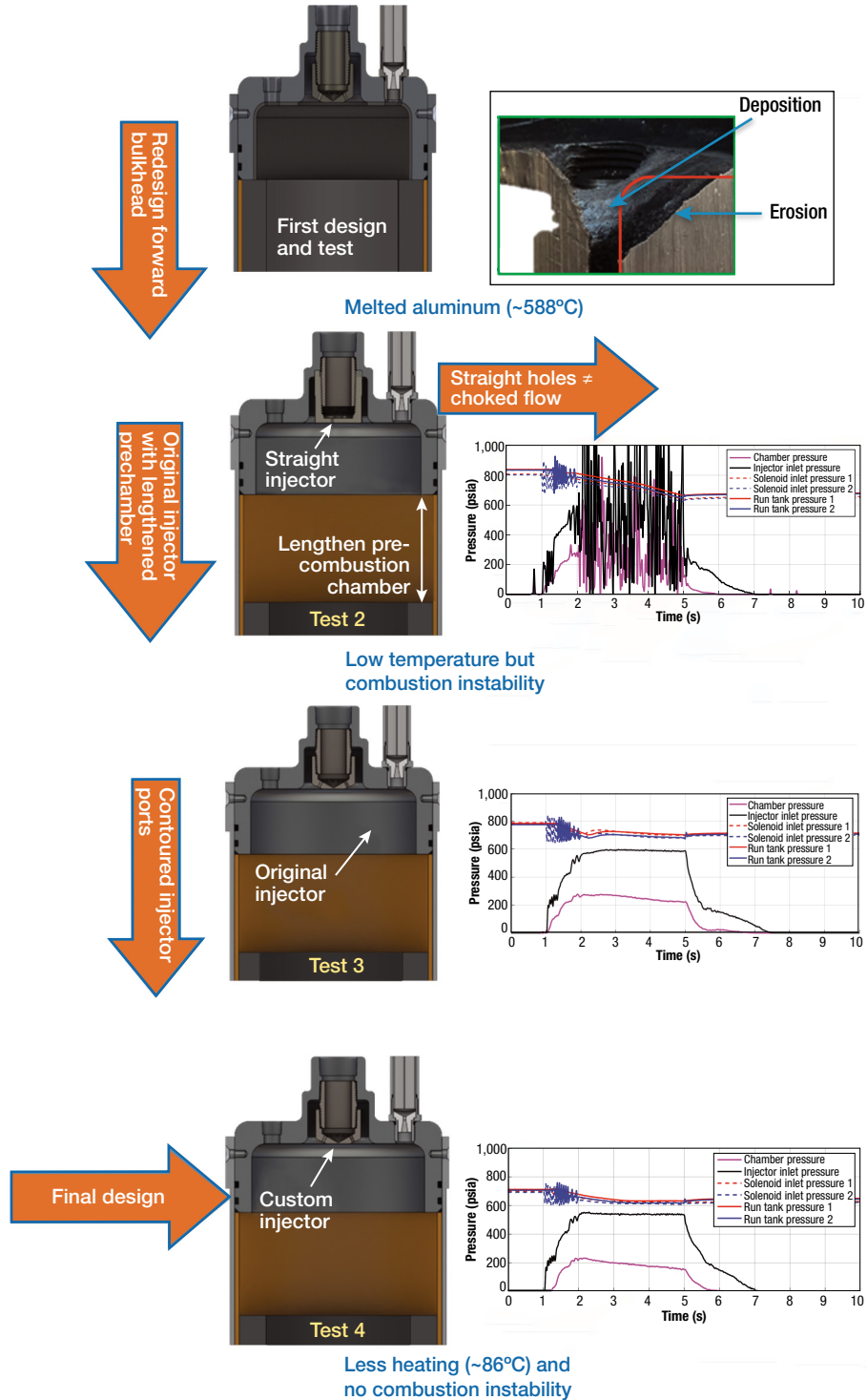


Figure 28. Summary of critical design features evaluated and flowchart of tests executed.

reusability of the hybrid rocket motor design. Through a series of four tests, we evaluated several design variations for the forward bulkhead geometry, injector, and precombustion chamber length to manage the thermal environment at and near the forward bulkhead of the motor. We conducted the test campaign to quickly discover geometric design features that reduced heating on the forward bulkhead. Between each test, we changed multiple variables, making it difficult to isolate the effects of each specific modification, but the information in total was useful. We found that the forward bulkhead heating is strongly dependent on the length-to-diameter ratio of the precombustion chamber, injector, and the forward-facing step of the fuel grain. During the test campaign, we designed a custom injector that helped reduce forward bulkhead heating along with chamber instabilities.

Near-term future work could explore how our iterative design changes affect forward bulkhead heating and overall hybrid motor performance. Longer-term future work in support of our overall reusable hybrid rocket motor vision could include testing the 400-lbf motor for the intended duration of 45 s to evaluate the bulkhead heating rate. Next steps could then include integration of all systems, evaluation of reignition and reusability, and eventually a flight test. In parallel, the motor could be scaled up to the desired 1500 lbf to prove out the hybrid rocket motor performance that is needed to reach hypersonic conditions with a payload less than 500 lbf.

ACKNOWLEDGMENTS: This work was funded by APL's Force Projection Sector as part of an independent research and development project for fiscal years 2017–2021. We thank Precision Strike Mission Area (PSMA) executive Kirk Shawhan and PSMA chief scientist Glenn Mitzel for their guidance and support. In addition, this article would not have been possible without the significant contributions from Brian McGrath, Stephen D'Alessio, and Ann Pollack.

REFERENCES

- ¹US Government Accountability Office, "Hypersonic weapons: DOD should clarify roles and responsibilities to ensure coordination across development efforts," GAO-21-378, GAO, Washington, DC, Mar. 2021, <https://www.gao.gov/assets/gao-21-378.pdf>.
- ²S. D. Walker, "High regression rate hybrid rocket fuel grains with helical port structures," master's thesis, Utah State University, 2015, <https://digitalcommons.usu.edu/etd/4618>.
- ³"Penn Hybrid Rocket." University of Pennsylvania. <https://sites.google.com/site/pennhybridrocket/how-do-hybrid-rocket-motors-work> (accessed Jun. 11, 2021).
- ⁴N. S. Uddanti, "Analysis of a hybrid rocket burn using generalized compressible flow," master's thesis, Embry-Riddle Aeronautical University, 2015, <https://commons.erau.edu/edt/285/>.
- ⁵B. J. McBride, M. J. Zehe, and S. Gordon, "NASA Glenn coefficients for calculating thermodynamic properties of individual species," NASA Glenn Research Center, Cleveland, OH, NASA TP-2002-211556, 2002, <https://ntrs.nasa.gov/citations/20020085330>.
- ⁶S. A. Whitmore, Z. W. Peterson, and S. D. Eilers, "Analytical and experimental comparisons of HTPB and ABS as hybrid rocket fuels," in *Proc. 47th AIAA/ASME/SAE/ASEE Joint Propulsion Conf. & Exhib.*, 2011, AIAA-2011-5909, <https://doi.org/10.2514/6.2011-5909>.
- ⁷R. W. Humble, G. N. Henry, and W. J. Larson, *Space Propulsion Analysis and Design, Space Technology Series*, ed. 1. Boston, MA: Learning Solutions, 2007.
- ⁸P. K. Nardozzo, S. Popkin, and J. R. Smith, "Feasibility study for hypersonic flight test using a reusable hybrid rocket motor," in *Proc. AIAA Propulsion and Energy 2019 Forum*, Indianapolis, IN, AIAA 2019-3838, <https://doi.org/10.2514/6.2019-3838>.
- ⁹M. Bouziane, A. E. M. Bertoldi, P. Milova, P. Hendrick, and M. Lefebvre, "Performance comparison of oxidizer injectors in a 1-kN paraffin-fueled hybrid rocket motor," *Aerosp. Sci. Technol.*, vol. 89, pp. 392–406, 2019, <https://doi.org/10.1016/j.ast.2019.04.009>.
- ¹⁰BETE SS12 Injector. https://www.bete.com/PDFs/BETE_SS.pdf (accessed Jun. 11, 2021).
- ¹¹W. Anderson and V. Yang, Eds., *Liquid Rocket Engine Combustion Instability* (Progress in Astronautics and Aeronautics Series, vol. 169). Reston, VA: American Institute of Aeronautics and Astronautics, Inc., 1995, <https://doi.org/10.2514/5.9781600866371.0000.0000>.
- ¹²M. J. Chiaverini and K. K. Kuo, *Fundamentals of Hybrid Rocket Combustion and Propulsion* (Progress in Astronautics and Aeronautics Series, vol. 218). Reston, VA: American Institute of Aeronautics and Astronautics, Inc., 2007, <https://doi.org/10.2514/5.9781600866876.0000.0000>.
- ¹³C. Carmicino and A. R. Sorge, "Influence of a conical axial injector on hybrid rocket performance," *J. Propulsion Power*, vol. 22, no. 5, pp. 984–995, Sep.–Oct. 2006, <https://doi.org/10.2514/1.19528>.
- ¹⁴G. P. Sutton and O. Biblarz, *Rocket Propulsion Elements*, 8th ed. Hoboken, NJ: Wiley, 2010.
- ¹⁵G. Story, "Chapter 10: Large-scale hybrid motor testing," Huntsville, AL: NASA Marshall Space Flight Center, 2006.
- ¹⁶H. Flaherty and N. O'Neill, "Design of minimally invasive method for combustion chamber pressure measurements in HTPB/N₂O hybrid rocket motors," https://www.colorado.edu/aerospace/sites/default/files/attached-files/hickam_aiaa.pdf.
- ¹⁷F. Heeg, L. Kilzer, R. Seitz, and E. Stoll, "Design and test of a student hybrid rocket engine with an external carbon fiber composite structure" *Aerospace*, vol. 7, no. 5, art. 57, 2020, <https://doi.org/10.3390/aerospace7050057>.
- ¹⁸US Department of Defense, *Metallic Materials and Elements for Aerospace Vehicle Structures*, MIL-HDBK-5J. Washington, DC: DOD, 2003.
- ¹⁹B. R. McKnight, "Advanced hybrid rocket motor propulsion unit for cubesats," master's thesis, Pennsylvania State University, Aug. 2015.
- ²⁰G. Zillac, B. S. Waxman, E. Doran, J. Dyer, M. A. Karabeyoglu, and B. Cantwell, "Peregrine hybrid rocket motor ground test results," in *Proc. AIAA Joint Propulsion Conf.*, Atlanta, GA, 2012, AIAA-2012-4017, <https://doi.org/10.2514/6.2012-4017>.
- ²¹O. Krauss, "Design and test of a lab-scale N₂O/HTPB hybrid rocket," AIAA, 2003.
- ²²Z. Arena, A. Althougies, and A. Rodulfo, "Hybrid rocket motor," bachelor's senior project report, California Polytechnic State University, Jun. 2010, <https://digitalcommons.calpoly.edu/aerosp/22>.
- ²³S. R. Gomes, L. Rocco, and J. A. F. F. Rocco, "Swirl injection effects on hybrid rocket motors," *J. Aerosp. Technol. Manage.*, vol. 7, no. 4, pp. 418–424, Nov. 2015, <https://doi.org/10.5028/jatm.v7i4.368>.
- ²⁴C. C. Jones, D. D. Myre, J. S. Cowart, "Performance and analysis of vortex oxidizer injection in a hybrid rocket motor," in *Proc. 45th AIAA/ASME/SAE/ASEE Joint Propulsion Conf. Exhib.*, Denver, CO, 2009, AIAA-2009-4938, <https://doi.org/10.2514/6.2009-4938>.
- ²⁵D. R. Tree, "Temperature, velocity and species profile measurements for reburning in a pulverized, entrained flow, coal combustor," US Department of Energy, Washington, DC, 1999, <https://doi.org/10.2172/7946>.
- ²⁶B. Waxman, "An investigation of injectors for use with high vapor pressure propellants with applications to hybrid rockets," doctoral dissertation, Stanford University, Jun. 2014, <https://searchworks.stanford.edu/view/10531747>.
- ²⁷C. Carmicino and A. R. Sorge, "Influence of a conical axial injector on hybrid rocket performance," *J. Propulsion Power*, vol. 22, no. 5, pp. 984–995, Sep.–Oct. 2006, <https://doi.org/10.2514/1.19528>.



Paige K. Nardozzo, Force Projection Sector, Johns Hopkins Applied Physics Laboratory, Laurel, MD

Paige K. Nardozzo, an Associate Professional Staff member at APL, is a propulsion technical lead. She has a BS in mechanical engineering from the Virginia Military Institute and an MS in mechanical engineering from Pennsylvania State University. Paige supports the reusable hybrid rocket motor described in this article as well as the Sea Based Terminal Future and Operational Fires programs. She has 4 years of experience at APL, primarily focused on rocket design, analysis, and testing. Her email address is paige.nardozzo@jhuapl.edu.



Justin R. Smith, Force Projection Sector, Johns Hopkins Applied Physics Laboratory, Laurel, MD

Justin R. Smith, a Senior Professional Staff member and assistant group supervisor at APL, is a project manager. He has a BS in mechanical engineering from Northern Arizona University and an MS in systems engineering from Johns Hopkins University. Justin supports the reusable hybrid rocket motor described in this article with analytical and hands-on experience in the field of aerospace and defense. He has over 12 years of aerospace engineering experience, with service at multiple industry-respected entities. His email address is justin.smith@jhuapl.edu.



Sarah H. Popkin, Air Force Office of Scientific Research, Wright-Patterson Air Force Base, OH

Sarah Popkin is now a program officer at the Air Force Office of Scientific Research. She has a BS, an MS, and a PhD in aerospace, aeronautical, and astronautical engineering, all from the University of Maryland, College Park. Over the last 13 years, Sarah has supported Department of Defense programs through aerodynamic modeling, wind tunnel testing, trajectory simulation, and basic research. She works to identify relevant research from around the world that can be used to solve critical challenges. Before joining the Air Force Office of Scientific Research, Sarah was a chief scientist in APL's Force Projection Sector where she developed annual calls for independent research and development (IRAD) proposals, worked with proposers to develop their research, and was a member of the IRAD panel that selects high-priority proposals for funding. Her email address is sarah.popkin@us.af.mil.



Joshua P. Higginson, Force Projection Sector, Johns Hopkins Applied Physics Laboratory, Laurel, MD

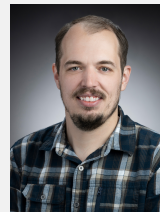
Joshua P. Higginson, a Senior Professional Staff member at APL, is a propulsion technical lead. He has a BS in aerospace engineering from Florida Institute of Technol-

ogy an MS in aeronautical and astronautical engineering from Purdue University. Josh supports the reusable hybrid rocket motor described in this article and is a project manager on a Defense Advanced Research Projects Agency (DARPA) rotating detonation engine program. He has 2 years of experience at APL and 6 years in the aerospace industry, primarily focused on rocket design, analysis, and testing, as well as mechanical design. His email address is josh.higginson@jhuapl.edu.



Marcus P. Musser, Force Projection Sector, Johns Hopkins Applied Physics Laboratory, Laurel, MD

Marcus P. Musser, a Senior Professional Staff member at APL, is a mechanical engineer. He has a BS in mechanical engineering from the University of Maryland, College Park. Marcus supports the reusable hybrid rocket motor described in this article and other hypersonic weapon programs including Air-Launched Rapid Response Weapon, Operational Fires, and Tactical Boost Glide. He has analytical and hands-on experience in the field of aerospace and defense, primarily in design, development, testing, and verification of complex systems for launch vehicles, satellites, and other payloads. He has been at APL for 5 years and has 10 years of experience at Orbital ATK. His email address is marcus.musser@jhuapl.edu.



Chuck E. Hebert, Force Projection Sector, Johns Hopkins Applied Physics Laboratory, Laurel, MD

Chuck Hebert, a Senior Professional Staff member at APL, is a mechanical engineer. He has a BS and an MS in mechanical engineering from the University of Maryland, Baltimore County. Chuck supports the reusable hybrid rocket motor described in this article, specializing in mechanical design for prototype and small-volume production. He is experienced in mechanical design and integration for air and ground vehicles, with over 10 years of experience. His email address is chuck.hebert@jhuapl.edu.

Gary Worrell, Force Projection Sector, Johns Hopkins Applied Physics Laboratory, Laurel, MD

Gary Worrell, a Senior Professional Staff member at APL, is a systems engineer. Gary supports the reusable hybrid rocket motor described in this article. He has 38 years of experience involving virtually every aspect of submarine navigation systems, including operation, maintenance, procedures, analysis, enhancement, training, and shipyard/predeployment underway support, with over 30 years of experience at APL and 10 in the US Navy.